Available online at www.sciencedirect.com
SCIENCE DIRECT
Journal of Power Sources 145 (2005) 652–658
JOURNAL OF POWER SOURCES
www.elsevier.com/locate/jpowsour

Effect of lithium carbonate on nickel catalysts for direct internal reforming MCFC

Jae-Suk Choi [a], Jung-Sook Yun [a], Heock-Hoi Kwon [b], Tae-Hoon Lim [c], Seong-Ahn Hong [c], Ho-In Lee [a,*]

[a] *School of Chemical and Biological Engineering and Research Center for Energy Conversion and Storage, Seoul National University, Seoul 151-744, Korea*
[b] *Department of Chemical and Environmental Engineering, Soongsil University, Seoul 156-743, Korea*
[c] *Fuel Cell Research Center, Korea Institute of Science and Technology, Seoul 136-791, Korea*

Accepted 13 December 2004
Available online 23 May 2005

Abstract

Despite many advantages of the direct internal reforming molten carbonate fuel cell (DIR-MCFC) in producing electricity, there are many problems to solve before practical use. The deactivation of reforming catalyst by alkali like lithium is one of the major obstacles to overcome. A promising method is addition of TiO_2 into the Ni/MgO reforming catalyst, which resulted in the increased resistance to lithium poisoning as we previously reported. To understand how added titania worked, it is necessary to elucidate the deactivation mechanism of the catalysts supported on metal oxides such as MgO and MgO–TiO_2 composite oxide.

Several supported nickel catalysts deactivated by lithium carbonate were prepared, characterized and evaluated. The Ni/MgO catalyst turned out to be most vulnerable to lithium deactivation among the employed catalysts. The activity of the Ni/MgO gradually decreased to zero with increasing amount of lithium addition. Deactivation by lithium addition resulted from the decrease of active site due to sintering of nickel particles as well as the formation of the $Li_yNi_xMg_{1-x-y}O$ ternary solid solution. These were evidenced by H_2 chemisorption, temperature programmed reduction, and XRD analyses. As an effort to minimize Li-poisoning, titanium was introduced to MgO support. This resulted in the formation of Ni/Mg_2TiO_4, which seemed to increase resistance against Li-poisoning.

Keywords: Deactivation by lithium; Ni/MgO; Ni/MgO–TiO_2; DIR-MCFC

1. Introduction

Among various types of fuel cells, the molten carbonate fuel cell (MCFC) is believed to be commercialized with highest possibility in near future. It is due to the fact that it has higher energy efficiency than conventional thermal power plants and can be supplied as a dispersive power source fueled by LNG or pre-treated coal gas. Based on the position of reformer the MCFC is generally classified into two types, internal and external reforming. The direct internal reforming MCFC (DIR-MCFC) takes advantage of thermal benefit by using exothermic heat of electrochemical reaction on anode for endothermic heat of reforming reaction. Consumption of exothermic heat makes MCFC operated without extra coolant possible. However, it is well known in DIR-MCFC that the reforming catalyst in the anode chamber easily deteriorated by alkali carbonate which had been transported via the vapor and/or creep of electrolyte.

For the reforming of natural gas to produce hydrogen, the nickel catalysts supported on silica, alumina, and magnesia have been currently used [1]. Among those catalysts, Ni/MgO catalyst has been widely investigated for DIR-MCFC [2–7]. Unfortunately, however, there are many obstacles to overcome to practically employ the Ni/MgO catalyst such as alkali poisoning. Moon et al. [6,7] reported the deactivation of the

* Corresponding author. Tel.: +82 2 880 7072; fax: +82 2 888 1604.
E-mail address: hilee@snu.ac.kr (H.-I. Lee).

0378-7753/$ – see front matter © 2005 Elsevier B.V. All rights reserved.
doi:10.1016/j.jpowsour.2004.12.066

Ni/MgO catalyst operated in DIR-MCFC single cell for 72 h. They suggested that lithium was the most notorious among the alkalis evaluated and that the deactivation might be due to chemical reactions of catalyst with lithium. As an effort to improve the resistance to Li-poisoning, we studied the use of composite oxides instead magnesia as supporting materials for nickel loading. The resistance of the catalyst to Li-poisoning drastically increased when titania was introduced to Ni/MgO catalyst [8]. The mechanism of Li-deactivation and reason for the high resistivity of the Ni/MgO–TiO_2 remained obscure.

In this paper, we prepared a series of supported nickel catalysts over MgO deactivated with varying amounts of lithium carbonate, and evaluated their catalytic properties. Characterization including N_2 physisorption, X-ray diffraction (XRD), and H_2 chemisorption was carried out to elucidate the role of lithium as a deactivating material and the role of the titania as a material giving resistance.

2. Experimental

2.1. Preparation of the catalysts

Magnesium oxide was prepared by calcining magnesium hydroxide at 973 K for 12 h. The nickel catalyst supported on MgO was abbreviated to NM. Synthetic procedure for MgO–TiO_2 composite oxides as a support is as follows. Magnesium acetate tetrahydrate (G.R., Junsei) and titanium tetraisopropoxide (G.R., Junsei) were dissolved in water and isopropyl alcohol, respectively. Corresponding precursor solution of titanium was dropped to the solution of magnesium acetate until target Mg/Ti ratios were achieved, and then aged for 3 h in ice-water bath. The target Mg/Ti ratios were 2, 1, and 0.5 which corresponds to qandilite (Mg_2TiO_4), geikielite ($MgTiO_3$) and karooite ($MgTi_2O_5$), respectively. After removing the solvent in the rotary evaporator, a mixture of powder and sticky gel was obtained. Then, the mixture was heated up to 973 K at 10 K min^{-1}, and calcined at 973 K for 12 h in air.

The active component, nickel, was loaded by incipient wetness method. The aqueous solution of nickel nitrate hexahydrate (99.9%, Aldrich) was injected into a dried support, and finished upon reaching the amount corresponding to 20 wt.% of nickel loading. After the impregnation precursors were dried at 383 K. Then, the supported nickel catalysts were oxidized in liquid phase with NaOCl for 12 h at 353 K [9]. The samples were filtered and washed using a large amount of deionized water and dried again.

2.2. Catalytic activity test and deactivation test

In order to study Li-poisoning, stability tests were carried out. The lithium carbonate powder (99%, Avondale Laboratories) was mechanically mixed with the catalysts, and then the mixture was treated at 923 K for 1 h in flowing hydrogen with 50% N_2 balance. Amount of Li_2CO_3 used was expressed in wt.% based on the weight of Li-free catalysts and denoted to xL-as prefix in catalyst codes. For example, 10LNM stands for the catalyst supported on MgO being mixed with 10 wt.% of Li_2CO_3.

The catalytic reactions were conducted in quartz tube reactor at 923 K under atmospheric pressure, the similar condition used actually in MCFC [10]. Athermowell equipped with a Ktype thermocouple was placed in the center of catalyst bed. A controlled amount of CH_4 and H_2O with molar ratio of 1:2.5 was fed into the reactor by a mass flow controller and a micro syringe, respectively. The flow rate of methane was 20 sccm. For each run, the same amount of active nickel in the poisoned catalysts was made to put in the reactor for the comparison of activity because the catalysts contained different contents of nickel after deactivation. Gaseous effluents were passed through a trap maintained at 273 K to remove the unreacted water and then analyzed by on-line gas chromatography (DS6200, Donam) equipped with a TCD detector using Ar as carrier gas.

2.3. Characterization

The powder X-ray diffraction (XRD) with a Mac Science M18XHF22-SRA diffraction spectrometer using Cu Kα as a radiation source was used to determine the phases of the prepared samples.

BET surface area and pore size distribution were determined by N_2 adsorption and desorption using a porosimetry analyzer (ASAP 2010, Micromeritics Corp.).

H_2-chemisorption was performed in home-made volumetric apparatus equipped with Baratron absolute pressure gauge and transducer (Type 121A and 122A, MKS) according to the procedure described elsewhere [11].

Elemental analysis was carried out on an inductively coupled plasma-atomic emission spectrometer (ICPS-7500, Shimadzu).

3. Results and discussion

3.1. Ni/MgO catalyst

Table 1 summarized the results of elemental analyses by induced coupled plasma (ICP) for the catalyst samples. The measured nickel loading for 0LNM was 19.2 wt.%. Almost all of the introduced lithium as Li_2CO_3 remained in the samples after calcination at 923 K regardless of lithium loading.

Table 1
Atomic composition of the catalysts deactivated by lithium carbonate

Atomic fraction (%)	0LNM	5LNM	10LNM	15LNM	20LNM
Li	0	4.2	10.2	14.0	17.2
Mg	86.0	82.3	77.1	74.0	71.1
Ni	14.0	13.5	12.7	12.1	11.6

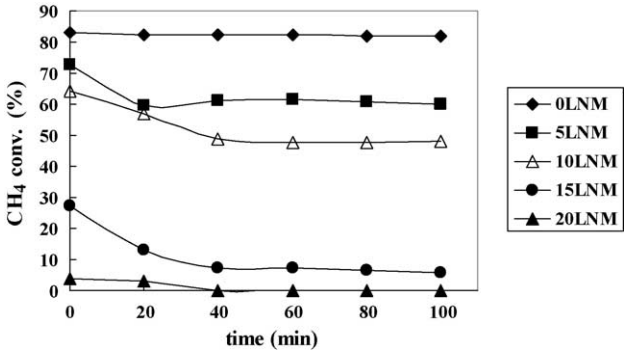

Fig. 1. Activity of deactivated catalysts in methane steam reforming by different amount of lithium. ◆: 0LNM; ■: 5LNM; △: 10LNM; ●: 15LNM; ▲: 20LNM.

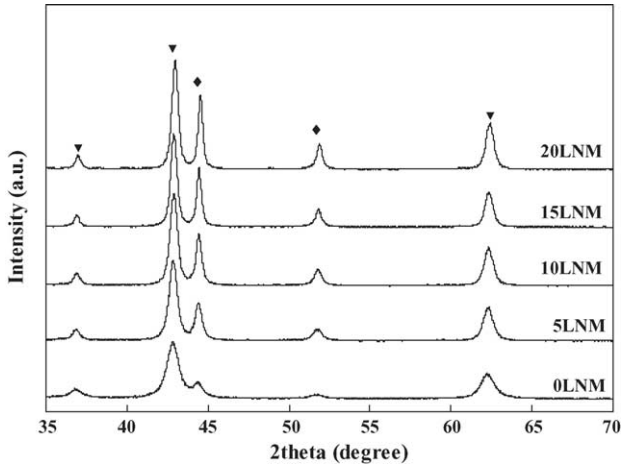

Fig. 2. XRD patterns of deactivated catalysts. ◆: Ni; ▼: support.

The prepared samples were evaluated using the steam reforming of methane and the time-on-stream data were shown in Fig. 1. The 0LNM catalyst experienced no deactivation by lithium showed a constant methane conversion of 83% for 4 h. For comparison, the conversions obtained at 100 min were evaluated for all the catalyst samples. As the amount of added lithium increased, the loss in catalytic activity also increased, implying that the catalyst was poisoned by lithium. For the 20LNM sample, the catalyst deactivated completely although there were small initial activity in induction period. Even though the simulated poisoning method by lithium applied in this paper are somewhat different from real poisoning process by lithium in the real stack of MCFC, comparing the results in Fig. 1 with the fact that Ni/MgO catalyst system gradually lose its activity as the system experience more lithium in the stack [4–6], we believe the simulated poisoning method emulate the catalyst deactivation considerably. On the contrary, in other study [12], an enhanced catalytic behavior by lithium in bio-ethanol steam reforming was reported when small fraction of lithium was added in Ni/MgO catalyst. Conventionally, lithium has been used as a catalytic promoter. Owing to this ambiguous behavior of lithium, there was no clear evidence to date that lithium directly deactivate and/or poison the Ni/MgO catalyst in the MCFC application.

In order to elucidate the effect of lithium on deactivating the Ni/MgO catalyst, the LNM catalysts were characterized using XRD and hydrogen chemisorption. The changes in crystalline phases after deactivation were identified by X-ray diffraction. Fig. 2 summarized X-ray diffraction patterns of the catalyst samples. Peaks of the support material and the reduced nickel were assigned. For all the samples, no significant new peaks were observed. This indicates that added lithium did not form any other crystalline phases. As the lithium amount in the sample was increased, the peaks for metallic nickel became sharper and more intense. We believe it is due to not only the development of crystallinity of metallic nickel but also the enlargement of nickel crystallite. According to Arena et al. [13,14] lithium possibly caused sintering by enhancing mobility of nickel on the partially molten MgO matrix in the view of solid-state chemistry.

The crystallite size for nickel and support calculated using Scherrer equation and the lattice parameter for the support were listed in Table 2. Comparing with the activity data in Fig. 1, the 0LNM catalyst with the crystallite size of 21.3 run showed the highest activity among the prepared catalyst samples. As increasing the amount of lithium in the sample the sizes of nickel became larger, implying crystal growth and/or sintering. For the supported metal particle, crystallite size can be regarded as particle size because a small metal particle less than a few tens of nanometer can be regarded as a single crystallite [15]. Consequently, decreasing the active surface area of nickel caused by crystallite size increase ought to be one of the reasons for activity declination of the catalyst. The transition of crystallite sizes and lattice parameters of MgO in Table 2 will be discussed later in detail.

Fig. 3 is a close-up XRD image of Fig. 2 from 61° to 63°. The peaks between 62° and 63° are assigned to be MgO (2 2 0) phase. The peaks significantly shifted to higher angle as the added lithium amount increased. Considering our samples were composed of Ni and Mg, the shift of peaks described as dotted line in Fig. 3 stands for having more character of NiO, positioned at 62.92° for NiO (2 2 0) from

Table 2
Results of XRD analyses for deactivated catalysts

	0LNM	5LNM	10LNM	15LNM	20LNM
Crystallite size of Ni (nm)[a]	21.3	23.6	26.4	28.0	29.9
Crystallite size of support (nm)[b]	9.9	14.0	15.7	18.1	18.3
Lattice parameter (*a*)	4.214	4.212	4.210	4.209	4.206

[a] Calculated from the line broadening of Ni (1 1 1) peak.
[b] Calculated from the line broadening of MgO (2 2 0) peak.

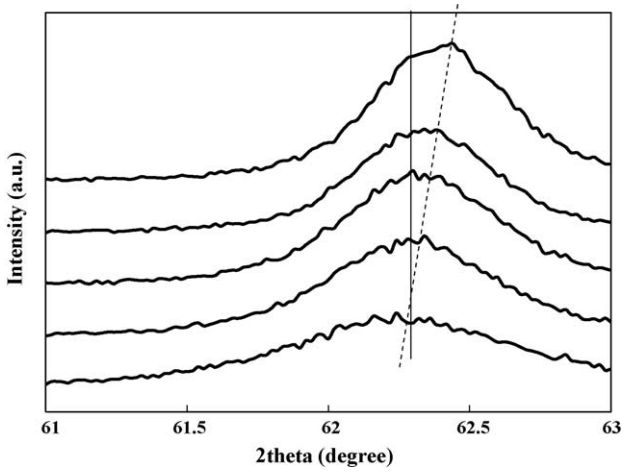

Fig. 3. A close-up image of XRD patterns of deactivated catalysts between 61° and 63°.

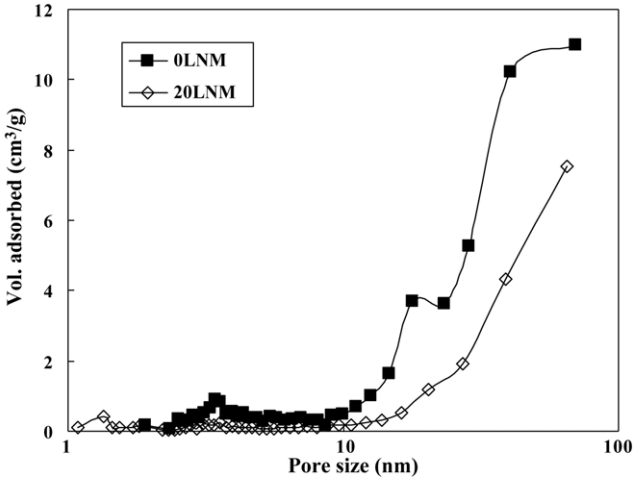

Fig. 4. Pore size distributions of catalysts. ■: 0LNM; ◇: 20LNM.

the reference [16] in the Li-containing support materials. The reduction of lattice parameters in Table 2 is another description for the same observation. It is resulted from the formation of a solid solution, leading more compact crystallite due to insertion of smaller Ni atom into lattice. It is well known that NiO and MgO form an ideal $Ni_xMg_{1-x}O$ solid solution, without NiO and/or MgO phase segregation, over the whole atomic fraction range [17]. In general, the peak shift plays an important role on judging the formation of solid solution in catalyst study. Arena et al. [18] prepared a series of NiO–MgO samples calcined at different temperatures in air for 16 h and carried out XRD measurements using a high-resolution powder diffactometer with monochromatized non-doublet synchrotron radiation. Resultantly, it was observed that the peaks for MgO phases distinguished from those for NiO phases shifted to higher angles with increasing calcination temperatures. They stated that the peak shift was attributed to the formation of solid solution. It was suggested that the more mobile nickel diffused into the support matrix with increasing calcination temperatures. In other papers [13,14], the impregnated lithium up to 1 wt.% was suggested to accelerate dissolving the supported nickel at high temperature calcination in both reducing and oxidizing conditions.

In contrast, Antolini [19] maintained that thermal treatment of Li-doped Ni/MgO gave rise to the formation of the ternary lithium nickel magnesium oxide ($Li_yNi_xMg_{1-y-x}O$) even though only a very small amount of Li^+ ions could enter MgO lattice without nickel. In the presence of nickel, however, the amount of lithium dissolved in MgO could remarkably increase, as Ni^{3+} ions could behavior as charge-compensating species. Moreover, he suggested an equation that can correlate the lattice parameter, a, of the ternary solid solution with the atomic fractions of Li, Ni and Mg:

$$a = a_0 - k(1 - x_{Mg})x_{Li} \quad (1)$$

where x_{Mg} and x_{Li} stand for the atomic fractions of Mg and Li, respectively, and a_0 for lattice constant.

In our XRD data in Fig. 3, it was almost impossible to de-convolute the XRD peaks into those for MgO and NiO. Considering the facts that it is very difficult for the supported metallic nickel being oxidized in the hydrogen rich condition applied in this study and that Li facilitates formation of the ternary solid solution in the presence of nickel as fully discussed above, the formation of $Li_yNi_xMg_{1-y-x}O$ must be a more plausible reason for XRD peak shift observed in Fig. 3.

Since the crystallite size of support material increased with increasing amount of lithium (Table 2), one may expect decrease of BET surface areas of the samples as suggested by Serra et al. [16]. Accordingly, the measured BET surface area of 42.5 $m^2\,g^{-1}$ for 0LNM decreased to that of 18.3 $m^2\,g^{-1}$ for 20LNM. The pore size distributions were depicted for comparison in Fig. 4. Both samples turned out to be mesoporous materials. Comparing the pore size distribution of 20LNM with that of 0LNM, pore volume in the range of 10–100 nm decreased significantly, which is consistent with crystallite sintering data in Table 2. Conclusively, addition of Li to Ni/MgO samples resulted in the formation of the ternary solid solution and simultaneously modified the morphology of the samples.

In order to confirm the formation of the ternary solid solution by addition of lithium to Ni/MgO catalyst system, the information on dispersion and particle size of supported nickel was essential. That information was obtained from hydrogen uptake data in Table 3. It is well known that atomic hydrogen is ready to adsorb on the reduced Ni surface [10,12]. Nickel

Table 3
Results of hydrogen chemisorption for deactivated catalysts

	0LNM	5LNM	10LNM	15LNM	20LNM
H_2 uptake ($\mu mol\ g_{cat}^{-1}$)	56.39	39.67	29.80	24.50	9.791
Dispersion (%)[a]	3.45	2.45	1.86	1.56	0.62
Size (nm)[b]	28.2	39.7	52.1	62.4	156

[a] Dispersion was calculated assuming that all of the nickel was reduced.
[b] Size was calculated using the equation from Ref. [20].

dispersion (D) was calculated using Eq. (2) by assuming that hydrogen chemisorbs dissociatively on nickel surface and that each hydrogen atom chemisorbs on each nickel atom:

$$D(\%) = \mathrm{Ni_{surf}}/\mathrm{Ni_{red}} \quad (2)$$

where $\mathrm{Ni_{surf}}(\mathrm{g_{cat}^{-1}})$ is the number of nickel atoms on the surface of the samples, which is counted by the number of hydrogen atoms and $\mathrm{Ni_{red}}$ ($\mathrm{g_{cat}^{-1}}$) is the number of the reduced nickel atoms. In Table 3, we assumed all of supported nickel (19.2 wt.%) would be reduced regarding severe reduction condition of 923 K and 50% H_2 with N_2 balance. The Ni mean particle size, d_s, was derived using the Eq. (3):

$$d_s(\mathrm{nm}) = 97.1/D(\%) \quad (3)$$

as suggested by Bartholomew et al. [20], where nickel particles were assumed to form hemisphere with various diameters. Comparing the nickel size data listed in Tables 2 and 3, where the similar data were collected by XRD and H_2 chemisorption, respectively, the mean sizes of supported nickel showed deviation with different degrees. More lithium introduced to the Ni/MgO samples resulted in more deviation in nickel size data. We believe that this discrepancy is originated from the assumption that all of the supported nickel was reduced. As we already mentioned from the XRD peak shift that lithium facilitated the formation of the solid solution of $\mathrm{Li}_y\mathrm{Ni}_x\mathrm{Mg}_{1-x-y}\mathrm{O}$, some fraction of supported nickel must be oxidized to form the solid solution. This would make the assumption of the complete reduction of supported nickel invalid. Hence, we decided to consider the degree of reduction, α, defined as in Eq. (4):

$$\alpha = \mathrm{Ni_{red}}/\mathrm{Ni_{total}} \quad (4)$$

where $\mathrm{Ni_{total}}$ ($\mathrm{g_{cat}^{-1}}$) is the total number of supported nickel in the catalyst.

The degree of reduction can be derived from Eqs. (2) and (3) assuming that the particle size of supported nickel is identical to the crystallite size calculated by XRD data. This assumption is usually acceptable for a small size of supported metals [15]:

$$a = (d_s)(\mathrm{Ni_{surf}})/(97.1)(\mathrm{Ni_{total}}) \quad (5)$$

If we deduce the degree of reduction from the experimental data, the supported nickel can be classified into metallic nickel and oxidized nickel in solid solution. Table 4 listed the calculated data using Eq. (5). In the case of 20LNM, over 80% of nickel was believed to be dissolved in the ternary solid solution, which resulted in the loss of active site, reduced nickel surface. This explains well the loss of activity for the 20LNM and the trend of less activity of the catalyst samples with increasing lithium addition. The atomic fractions of each component for the Li-poisoned catalysts with varying lithium amount were measured by ICP analysis and summarized in Table 1. Combining these results with the degree of reduction, the composition of ternary solid solution produced after Li-poisoning can be estimated assuming that all of detected lithium by ICP participated in the formation of solid solution. The re-calculated atomic fractions of each metal were shown in the lower part of Table 4. This estimated atomic fraction in the ternary solid solution was applied to the Eq. (1) to confirm the validity of the previous assumptions that all of the detected lithium participated in the ternary solid solution. In Fig. 5, $(1-x_{\mathrm{Mg}})x_{\mathrm{Li}}$ was plotted to the lattice parameter of each sample listed in Table 2. There exists almost linear relationship between lattice parameter and the atomic fraction, implying that the detected lithium to the Ni/MgO samples participated in the formation of the ternary solid solution and that lithium facilitated the dissolution of nickel species into the solid solution, resulting in losing their activities. This indication also justifies our corresponding assumptions and validates our discussion. In addition, irreducible nickel species are known not to catalyze the steam reforming of methane [21,22]. In our previous report [8], it was found that once nickel formed the solid solution with MgO, the oxidized nickel required as high as 973 K to be reduced. Forming more solid solution resulted in higher reduction temperature. Since the reaction temperature employed in this paper is 923 K, the nickel in solid solution could not be reduced, and

Table 4
List of atomic composition of deactivated catalysts and $\mathrm{Li}_y\mathrm{Ni}_x\mathrm{Mg}_{1-x-y}\mathrm{O}$ ternary solid solution

	0LNM	5LNM	10LNM	15LNM	20LNM
Degree of reduction (%)	75.63	58.96	49.53	43.19	18.43
Atomic fraction in catalyst (%)					
Metallic Ni	10.6	7.94	6.28	5.22	2.15
Oxidized Ni	3.42	5.53	6.40	6.87	9.45
Li	0	4.24	10.2	14.0	17.2
Mg	86.0	82.3	77.1	74.0	71.1
Atomic fraction in $\mathrm{Li}_y\mathrm{Ni}_x\mathrm{Mg}_{1-x-y}\mathrm{O}$ solid solution (%)					
Ni	3.83	6.00	6.82	7.25	9.80
Li	0	4.75	12.4	17.9	23.7
Mg	96.2	89.5	82.3	78.0	66.5

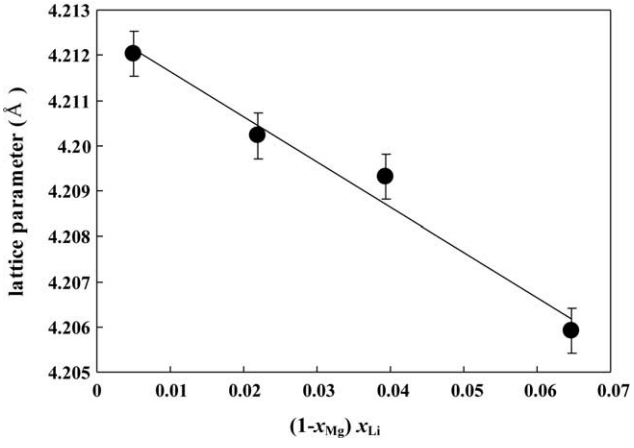

Fig. 5. Plot of lattice parameter vs. $(1-x_{\mathrm{Mg}})x_{\mathrm{Li}}$. Closed circles stand for the values for the present $\mathrm{Li}_y\mathrm{Ni}_x\mathrm{Mg}_{1-x-y}\mathrm{O}$ samples. x_{Mg}, x_{Li}: atomic fraction of Mg and Li in ternary solid solution, respectively.

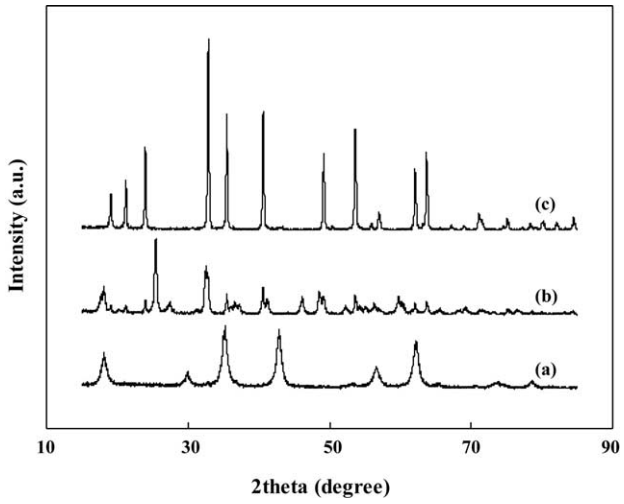

Fig. 6. XRD patterns of MgO–TiO_2 composite oxides. (a) Mg_2TiO_4, (b) $MgTi_2O_5$, and (c) $MgTiO_3$.

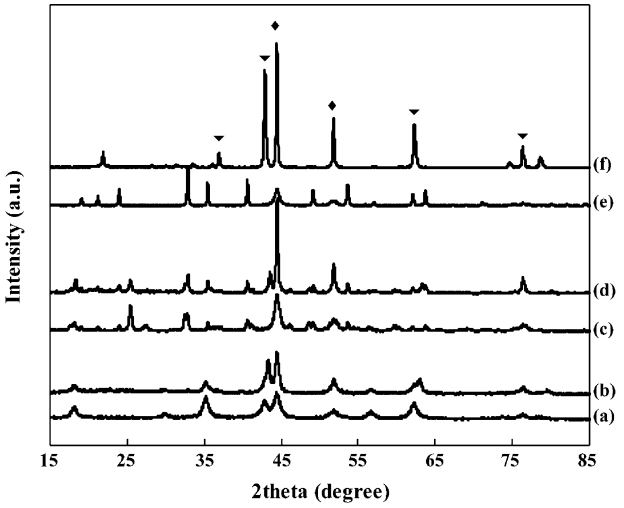

Fig. 7. XRD patterns of Ni/MgO–TiO_2 catalysts before and after deactivation. (a) NM_2T, (b) $20LNM_2T$, (c) NMT_2, (d) $20LNMT_2$, (e) NMT, and (f) 20LNMT; ◆: Ni; ▼: $Li_yNi_xMg_{1-x-y}O$.

thus could not participate in steam reforming. Considering this fraction of oxidized nickel in the solid solution and XRD peak shift, we propose that the formation of the ternary solid solution accelerated by lithium addition was the main reason for the deactivation of the Ni/MgO catalysts.

3.2. Deactivation of Ni/MgO–TiO_2 composite oxide

Since the solubility increase of nickel by lithium to form the solid solution is believed to be the major factor of deactivation, the support materials need to be substituted by the materials with more resistance to Li-poisoning. As a strong candidate, MgO–TiO_2 composite oxides were prepared and evaluated in our previous report [8]. For further investigation on deactivation mechanism for this composite oxide supports, three crystalline phases of MgO–TiO_2 with varying metal composition were prepared and analyzed.

The molar ratios of Mg to Ti for the prepared samples were 2:1,1:2, and 1:1, and their XRD patterns were shown in Fig. 6a–c, respectively. Each XRD pattern was well matched to that of qandilite (Mg_2TiO_4), karooite ($MgTi_2O_5$) and geikielite ($MgTiO_3$). Only the prepared sample made with the molar ratio of Mg to Ti to be 1:2 had some peaks of geikielite with low intensity.

After nickel was introduced to the prepared composite oxides by following the same procedure, activity test was carried out with and without Li-poisoning and the results were summarized in Table 5. The T of the catalyst code represents titanium in the support and the numbers after M and T stand for molar ratio of Mg to Ti. Three different Li-free catalysts showed the methane conversions similar to that of the Ni/MgO catalyst. However, when the catalysts poisoned with 20 wt.% of lithium carbonate, only 20LNM2T sample maintained its original catalytic activity. Ni/$MgTiO_3$ lost almost of its activity. Ni/$MgTi_2O_5$ catalyst sustained only small fraction of its original activity. This indicates that composite oxides of magnesium and titanium are resistant to Li-poisoning and that there are optimum Mg to Ti ratio in minimizing Li-poisoning. This is a consistent result with our previous report [8].

Introduction of lithium to each catalyst resulted in the sintering of supported nickel. It was observed in Fig. 7 that the peaks for metallic nickel in the X-ray diffractogram became thinner and sharper after the deactivation by lithium. The degrees of sintering were different with the molar ratio of Mg to Ti in the support materials. In the cases of NMT_2 and NMT which were easily deactivated, it is clearly shown that the intense and sharp nickel peaks were emerged in Fig. 7d and f. On the other hand, the addition of lithium into the catalyst of NM_2T did not affect the peaks for the supported nickel significantly (Fig. 7b), which would be indicative of stronger resistance of NM_2T than those of the others. With respect to the crystalline structures of the supports, there is something worth being noticed. As seen in Fig. 7f, the structure of the weakest catalyst NMT was completely transformed into the structure of ternary solid solution $Li_yNi_xMg_{1-x-y}O$ after deactivation. It implies that the affinity to form the ternary solid solution caused by Li is much stronger than the tendency to maintain the magnesia-titania composite oxide. Considering that the crystalline structures of the other catalysts containing Ti were preserved after deactivation, the lowest activity

Table 5
Activities of the prepared Ni reforming catalysts supported on various MgO–TiO_2 composite oxides before and after Li poisoning

	NMT	20LNMT	NMT_2	$20LNMT_2$	NM_2T	$20LNM_2T$
CH_4 conversion (%)	80.7	5.52	64.5	13.3	78.0	77.6

of 20LNMT was ascribed to the less stability of its support to Li. It seemed that the affinities of composite oxides for the ternary solid solution might be the main origin of the different resistance to Li-poisoning. However, we cannot rule out the other possibilities such as the morphology of the catalyst including the particle sizes of both nickel and support, and nickel-support interactions varying with the ratio of Mg to Ti, which were mentioned previously [8]. In order to elucidate the role of titania, all of above things should be considered simultaneously. Further investigation is being carried out.

4. Conclusions

The effect of lithium carbonate on nickel reforming catalyst supported on MgO for DIR-MCFC was investigated. The more the amount of lithium carbonate added to the Ni/MgO catalyst, the more the catalyst deactivated. When 20 wt.% of lithium carbonate was added, the Ni/MgO catalyst lost all of its activity. Considering the XRD peak shift for lithium deactivated samples, the faction of oxidized nickel in samples calculated from hydrogen chemisorption, and higher reduction temperatures for Li-deactivated samples, we believe that the deactivation was due to the loss of active site, the surface of reduced nickel, resulted from the formation of $Li_yNi_xMg_{1-x-y}O$ solid solution induced by lithium. To inhibit the dissolution of nickel, alternative material such as $MgO–TiO_2$ composite oxide was substituted for MgO. Resultantly, it was found that the Mg–Ti composite oxides were resistant to Li-poisoning and that there exists an optimum ratio of Mg to Ti in minimizing Li-poisoning. The formation of Ni/Mg_2TiO_4 seemed to be essential to increase resistance against Li-poisoning.

Acknowledgements

This work was financially supported by the Korea Electric Power Research Institute through the Korea Institute of Science and Technology, and by the Korea Science and Engineering Foundation through the Research Center for Energy Conversion and Storage.

References

[1] J.R. Rostrup-Nielsen, in: J.R. Anderson, M. Boudart (Eds.), Catalysis, vol. 5, Springer-Verlag, Berlin, 1984, pp. 1–117.
[2] S. Cavallaro, S. Freni, R. Cannistraci, M. Aquino, N. Giordano, Int. J. Hydrogen Energ. 17 (1992) 181–186.
[3] R.J. Berger, E.B.M. Doesburg, J.G. van Ommen, J.R.H. Ross, Appl. Catal. A: Gen. 143 (1996) 343–365.
[4] M. Matsumura, C. Hirai, Ind. Eng. Chem. Res. 37 (1998) 1793–1798.
[5] M. Matsumura, C. Hirai, J. Chem. Eng. Jpn. 31 (1998) 734–740.
[6] H.-D. Moon, T.-H. Lim, H.-I. Lee, Bull. Kor. Chem. Soc. 20 (1999) 1413–1417.
[7] H.-D. Moon, J.-H. Kim, H.Y. Ha, T.-H. Lim, S.-A. Hong, H.-I. Lee, J. Kor. Ind. Eng. Chem. 10 (1999) 754–760.
[8] J.-S. Choi, H.-H. Kwon, T.-H. Lim, S.-A. Hong, H.-I. Lee, Catal. Today 93–95 (2004) 553–560.
[9] K.S. Jung, B.-Y. Coh, H.-I. Lee, Bull. Kor. Chem. Soc. 20 (1999) 89–94.
[10] Y.J. Shin, H.-D. Moon, T.-H. Lim, H.-I. Lee, Stud. Surf. Sci. Catal. 130 (2000) 431–436.
[11] C.H. Batholomew, in: Z. Paál, P.G. Menon (Eds.), Hydrogen Effect in Catalysis, Marcel Dekker Inc., New York, 1988, pp. 139–165.
[12] F. Frusteri, S. Freni, V. Chiodo, L. Spadaro, O. Di Blasi, G. Bonura, S. Canallaro, Appl. Catal. A: Gen. 270 (2004) 1–7.
[13] F. Arena, F. Frusteri, L. Plyasova, A. Parmaliana, J. Chem. Soc. Faraday Trans. 94 (1998) 3385–3391.
[14] F. Arena, A.L. Chuvilin, A. Parmaliana, J. Phys. Chem. 99 (1995) 990–998.
[15] J.W. Geus, in: Z. Paál, P.G. Menon (Eds.), Hydrogen Effect in Catalysis, Marcel Dekker Inc., New York, 1988, pp. 85–116.
[16] M. Serra, P. Salagre, Y. Cesteros, F. Medina, J.E. Sueiras, Solid State Ionics 134 (2000) 229–239.
[17] T. Yoshida, T. Tanaka, H. Yoshida, T. Funabiki, S. Yoshida, J. Phys. Chem. 100 (1996) 2302–2309.
[18] F. Arena, F. Frustrei, A. Parmaliana, L. Plyasova, A.N. Shmakov, J. Chem. Soc., Faraday Trans. 92 (1996) 469–471.
[19] E. Antolini, Mater. Lett. 51 (2001) 385–388.
[20] C.H. Bartholomew, R.B. Pannell, J.L. Butler, J. Catal. 65 (1980) 335–347.
[21] F. Arena, B.A. Horrell, D.L. Cocke, A. Parmaliana, N. Giordano, J. Catal. 132 (1991) 58–67.
[22] A. Parmaliana, F. Arena, F. Frusteri, S. Coluccia, L. Marchese, G. Martra, A.L. Chuvilin, J. Catal. 141 (1993) 34–47.